PCCP

Towards reliable ab initio sublimation pressures for organic molecular crystals – Are we there yet?

Journal:	*Physical Chemistry Chemical Physics*
Manuscript ID	CP-ART-03-2019-001572.R2
Article Type:	Paper
Date Submitted by the Author:	01-Jun-2019
Complete List of Authors:	Cervinka, Ctirad; University of Chemistry and Technology, Prague, Beran, Gregory; University of California Riverside, Chemistry
Note: The following files were submitted by the author for peer review, but cannot be converted to PDF. You must view these files (e.g. movies) online.	
toc1.TIF	

Towards reliable ab initio sublimation pressures for organic molecular crystals – Are we there yet?

Ctirad Červinka [†,*], *Gregory Beran* [‡]

[†] Department of Physical Chemistry, University of Chemistry and Technology Prague, Technická 5, CZ-166 28 Prague 6, Czech Republic

[‡] Department of Chemistry, University of California, Riverside, California 92521, United States

*Corresponding author: cervinkc@vscht.cz

ABSTRACT.

Knowledge of molecular crystal sublimation equilibrium data is vital in many industrial processes, but this data can be difficult to measure experimentally for low-volatility species. Theoretical prediction of sublimation pressures could provide a useful supplement to experiment, but the exponential temperature dependence of sublimation (or any saturated vapor) pressure curve makes this challenging. An uncertainty of only a few percent in the sublimation enthalpy or entropy can propagate to an error in the sublimation pressure exceeding several orders of magnitude for a given temperature interval. Despite this fundamental difficulty, this paper performs some of the first *ab initio* predictions of sublimation pressure curves. Four simple molecular crystals (ethane, methanol, benzene, and imidazole) have been selected for a case study showing the currently achievable accuracy of quantum chemistry calculations. Fragment-based *ab initio* techniques and the quasi-harmonic approximation are used for calculations of cohesive and phonon properties of the crystals, while the vapor phase is treated by the ideal gas model. *Ab initio* sublimation pressure curves for model compounds are compared against their experimental counterparts. The computational uncertainties are estimated, weak points of the computational methodology are identified, and further improvements are proposed.

1. INTRODUCTION

Data on sublimation and vaporization equilibrium of molecular crystals play a significant role in processes such as epitaxial technologies, crystal engineering, separation techniques, solvent design, solvation of drug molecules, and environmental modeling of pollutant distribution as most of the chemical compounds involved in such processes form molecular crystals. The accurate experimental determination of sublimation and vaporization data for low-volatility compounds is very difficult. It is not unusual for measurements made by different methods or laboratories to differ by tens of percent or even orders of magnitude.[1] Reliable saturated vapor pressures down to the micropascal regime can be obtained by thermodynamically controlled extrapolation of sublimation pressures obtained in the "measurable" pressure range.[2-4] This method requires knowledge of several properties which are generally not available for many compounds, including heat capacities of condensed and gaseous phases or general molecular parameters such as the dipole moment. Existing empirical estimation methods for evaluation of heat capacities work quite reliably.[5, 6] However, estimates of vapor pressure data, such as those based on group contribution concept,[7, 8] quantitative structure-property relationship[9] or theorem of corresponding states[10, 11] may exhibit large errors. A reliable *ab initio* predictive methodology could thus help to fill the gaps in availability of data on sublimation equilibrium, especially for molecular crystals whose crystal packing is governed by a delicate interplay of noncovalent interactions that can be reliably modeled by means of theoretical chemistry.

Sublimation equilibrium can be in principle studied *ab initio*, using computational methods of quantum chemistry and statistical thermodynamics. Predicted ideal gas thermodynamic properties are fairly reliable for most organic molecules, with computational uncertainties in the isobaric heat capacity and entropy not exceeding 2 % (even less for rigid molecules), as shown by Červinka et al.[12-14] In the solid phase, it has become a rather straightforward task to calculate the cohesive energy of a small-molecule molecular crystal within the chemical

accuracy (~4 kJ/mol) at an acceptable computational cost, using either fragment based many body approaches[15-20] or periodic quantum calculations.[21-28] State-of-the-art computational methodologies approach even the sub-kJ·mol^{-1} accuracy for crystals of smaller molecules, as evidenced by the recent work of Hirata et al. for carbon dioxide,[29] of Yang et al.[30] for benzene and our work on polymorphism of methanol.[31, 32] Phonon and thermodynamic properties of molecular crystals at finite temperatures and pressures have become computationally accessible recently thanks to the versatile (yet imperfect) quasi-harmonic approximation,[33, 34] which is capable of describing the thermal expansion of crystals and related anharmonic phenomena with a reasonable accuracy.[31-33, 35-42] More elaborate treatments of anharmonicity based on the vibrational self-consistent field model and subsequent corrections, being considerably more involved,[43-45] are as such beyond the scope of this work.

Combining all these building blocks enables prediction of the temperature-dependent sublimation enthalpy ($\Delta_{vap}H$) with an uncertainty of roughly 10 %.[46] This uncertainty often corresponds to chemical accuracy (1 kcal/mol or 4 kJ/mol) and represents a reasonable agreement between theory and experiment. However, the presence of a 10 % uncertainty in $\Delta_{vap}H$ in the exponent of the formula leading to the saturated sublimation pressures ($p_{sub}^{\varnothing}$) can translate to disastrous errors amounting to several orders of magnitude. Accordingly, few attempts to predict $p_{sub}^{\varnothing}$ from first principles can be found in literature.[29, 40, 41, 47] The prediction of the normal sublimation temperature of carbon dioxide to within a few Kelvin of experiment by the Beran group[40] can be regarded as a success of the computational chemistry, even though this agreement occurred mainly due to a fortuitous compensation of errors in the calculated cohesive and thermal energies of the crystalline phase. Červinka and Fulem[41] demonstrated for a set of 20 simple molecular crystals that at present, first-principles calculations of $p_{sub}^{\varnothing}$ should be regarded as successful when the calculated $p_{sub}^{\varnothing}$ has the same order of magnitude as the experimental counterpart over a broad temperature interval.

To investigate the performance of the state-of-the-art calculations, four simple organic molecular crystals with different structures, cohesive forces, and volatility (low temperature phases of ethane, methanol, benzene, and imidazole) have been selected here, and a comparative case study of ab initio $p_{\mathrm{sub}}^{\varnothing}$ calculations has been performed. These simple crystals were chosen because of both the availability of quality experimental data and because their small molecular sizes enable benchmark calculations to be performed with high-level correlated wavefunction techniques, including large-basis coupled cluster singles, doubles, and perturbative triples. The performance of several modern quantum mechanical levels of theory is compared against these benchmarks and/or experiment for the crystal structure optimizations and subsequent calculations of the cohesive energies, phonons, and sublimation properties of the crystals. We demonstrate that computational strategies combining the state-of-the-art electronic structure methods, quasi-harmonic treatment of phonons and the ideal-gas model are capable of predicting sublimation pressures to within an order of magnitude, in accord with the aforementioned criterion for successful predictions.

2. COMPUTATIONAL METHODS

Vapor phases here were modeled as an ideal gas whose thermodynamic properties were calculated within the well-established the rigid rotor – harmonic oscillator (RRHO) model,[48] optionally corrected by the one-dimensional hindered rotor model (1D-HR)[49, 50] for any internal-rotation-like degrees of freedom (methyl rotations in methanol and ethane). Molecular parameters required in the given statistical-thermodynamic models (optimized molecular geometry and vibrational frequencies for RRHO, and barriers to internal rotation and reduced moment of inertia for 1D-HR) were calculated either at the MP2/aug-cc-pVTZ level of theory, or within the DFT framework using the PBE functional, the D3 dispersion correction[23] with Becke-Johnson[51] damping (PBE-D3(BJ)), and the split-valence 6-311+G(d,p) basis set.

TABLE 1

Experimental crystal structures used as input for all first-principles calculations in this work along with the quasi-harmonic unit-cell parameters calculated at the temperatures of determination of the experimental structure. Unit-cell parameters are given in Å and degrees.

Molecule	*Z*	Space group	CSD Refcode	Data set	*a*	*b*	*c*	*β*
Ethane	2	$P2_1/n$	ETHANE01	Experiment at 85 K [52]	4.226	5.623	5.845	90.41
				HMBI(C,A)@HMBI[a]	4.11	5.53	5.96	91.2
				HMBI(C,A)@DFT[b]	4.15	7.18	5.39	69.8
Methanol	4	$P2_12_12_1$	METHOL04	Experiment at 122 K[53]	4.647	4.929	9.040	90.00
				HMBI(C,A)@HMBI[a]	4.85	4.52	8.98	90.0
				HMBI(C,A)@DFT[b]	4.96	4.41	8.99	90.0
Benzene	4	Pbca	BENZEN15	Experiment at 298 K[54]	7.380	9.515	6.903	90.00
				HMBI(C,A)@DFT[b]	7.49	9.52	6.88	90.0
Imidazole	4	$P2_1/c$	IMAZOL21	Experiment at 298 K[55]	7.326	4.997	9.556	122.68
				HMBI(C,A)@DFT[b]	7.53	5.34	9.74	116.7

[a] Structure optimized with respect to quasi-harmonic Helmholtz energy, obtained for MP2/avtz+Amoeba HMBI geometries and phonons, with CCSD(T)/CBS+Amoeba HMBI refinement of the cohesive energy.
[b] Structure optimized with respect to quasi-harmonic Helmholtz energy, obtained for PBE-D3(BJ)/PAW geometries and phonons, CCSD(T)/CBS+Amoeba HMBI refinement of the cohesive energy.

All computations for the crystalline phases started from the experimentally determined crystal structures, illustrated in Figure 1, see Table 1 for details. Unit cells were first optimized with respect to the total electronic energy. For all crystals, the underlying electronic structure was treated using the VASP software[56] and periodic PBE-D3(BJ) calculations[23, 51] coupled with the projector augmented wave (PAW) technique,[57] hard PAW potentials,[58] 900 eV cut-off for the energy of the plane waves (700 eV for methanol), and with a Monkhorst-Pack type k-point mesh centered around the Γ-point.[59] The number of k-points along the inverse unit cell vectors were set to roughly 40/*a* k-points where *a* stands for the length of the unit cell vector in the corresponding direction.[33]

FIGURE 1. Crystal structures of ethane, methanol, benzene, and imidazole studied in this work.

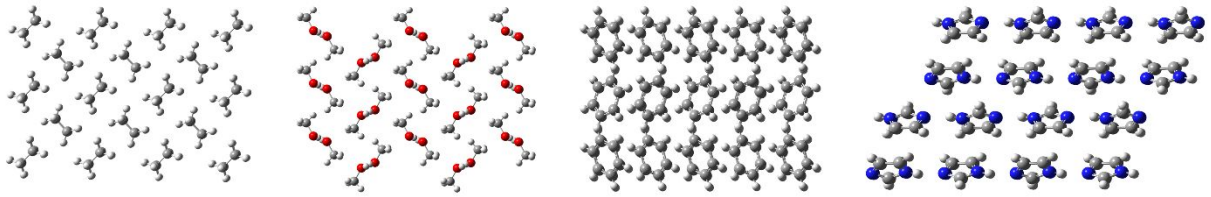

For comparison, the unit cell geometries of methanol and ethane were also optimized at the MP2 level using the hybrid many body interaction model (HMBI).[15, 60-62] HMBI expresses the total electronic energy of the unit cell in terms of a many body expansion that sums one-body (monomer), two-body (dimer) and many-body intermolecular contributions. One-body and shorter-range two-body interactions (intermolecular separations in the crystal within 10 Å) are treated at a higher-level quantum theory, while the longer-range two-body interactions (primarily long-range electrostatics) and many-body interactions (mostly induced dipoles due to molecular polarizability) are treated at a lower-level quantum theory or using a classical force field. For the crystalline geometry optimizations of ethane and methanol, perturbative MP2/aug-cc-pVTZ and the polarizable Amoeba force field[63] were used as the higher- and lower-level methods,[64] respectively. Tinker 6.2 was used to evaluate all Amoeba-based interaction energies.[65]

Having optimized the unit cell geometries, the computational protocol of the quasi-harmonic approximation was followed.[34] For the VASP DFT calculations, the volume dependence of the unit-cell electronic cohesive energies $E_{coh}(V)$ was modeled by scaling the vectors of the optimized cells by factors ranging from 0.95 to 1.08. Fixed-volume optimizations were then performed on these scaled unit cells. These calculations preserve the desired volume while allowing the unit cell parameters to relax anisotropically. Again, HMBI was also used to calculate the analogous MP2/aug-cc-pVTZ+Amoeba $E_{coh}(V)$ curves for ethane and methanol. Because the HMBI software package does not support fixed-volume optimizations, those unit cell optimizations were run under constant external pressures ranging from −0.45 GPa to +3.0

GPa.[31] In this manner, 15 and 13 points on the pseudo-anisotropic DFT-based and HMBI-based $E_{coh}(V)$ curves were computed, respectively. The resulting compression and expansion branches were fitted separately via the Murnaghan equation of state.[66] Its mathematical form ensures that the two branches are joint smoothly at the minimum of the $E_{coh}(V)$ curve.[31, 32]

For further refinement of the $E_{coh}(V)$ curves, single-point ab-initio HMBI calculations of unit-cell electronic energies were performed on the previously DFT-based optimized geometries (without any additional unit-cell optimization).[31, 38] Results of the contemporary gold standard quantum-chemical method, coupled cluster with iterative singles and doubles and perturbative triple excitations (CCSD(T)), extrapolated to the complete basis set (CBS),[67] were estimated by extrapolation of the MP2 triple-zeta and quadruple-zeta energies to the CBS and by subsequent addition of the quickly-convergent difference of CCSD(T) and MP2 energies evaluated in a smaller basis.[68] Specifically, this post-MP2 correlation correction was evaluated at the triple-zeta basis set for ethane and methanol, and at the double-zeta basis set for benzene and imidazole. HMBI energies were also computed with several other quantum chemistry models for comparison. The dispersion-weighted explicitly correlated version of the coupled cluster DW-CCSD(T)-F12,[69] coupled with the aug-cc-pVDZ basis set, denoted as the silver standard among the quantum-chemical methods,[70] was used. Next, two versions of dispersion-corrected MP2 were also used for comparison. These corrected MP2 models subtract the inappropriate uncoupled Hartree-Fock treatment of dispersion interactions from MP2 and add the coupled Kohn-Sham dispersion term based on either the time-dependent DFT and linear response theory (yielding the MP2C method[71]) or the semi-empirical dispersion term equivalent to Grimme's DFT-D3 model (yielding the MP2D method[72]). In case of MP2C, its bronze standard version (explicitly correlated MP2C-F12/aug-cc-pVDZ)[70] was used. For ethane and methanol, the CCSD(T)/CBS single-point calculations were also performed for the HMBI-based geometries. All the described ab initio wavefunction calculations were performed in Molpro.[73]

While the quantum mechanical one- and two-body terms in the HMBI energy capture the dominant interactions in the crystal, the many-body contributions are generally non-trivial. To assess the appropriateness of the classical polarizable force-field Amoeba for evaluation of the many-body interaction term, it was compared with periodic Hartree-Fock (pHF) treatment. The pHF calculations were performed with the pob-TZVP basis set[74] in the CRYSTAL14 code.[75] Replacing the Amoeba many-body treatment with a pHF one has helped improve the predictions in several earlier studies on small-molecule crystals.[32, 38]

Next, phonon properties were calculated using the finite-displacement method for unit-cells replicated to supercells (with size exceeding 10 Å in all directions) as implemented in the code Phonopy. To model the dependence of phonons on unit-cell volume, phonons were computed for 5 volumes around the minimum of the $E_{coh}(V)$ curve. In all cases, the harmonic phonon frequencies were computed on optimized geometries with the same model chemistry as was used to optimize the geometry, ensuring stationarity of the energy as required for the harmonic approximation. The vibrational Helmholtz energies A_{vib} were computed as a function of temperature and volume using the phonon density of states for each system. The dependence of A_{vib} on volume at the individual temperatures was fitted by a quadratic polynomial which is appropriate for interpolating within the range of calculated A_{vib} data points. However, it should not be used for extrapolations of A_{vib} to larger unit-cell volumes that were not covered by the phonon calculations.

The total Helmholtz energy of the crystal was obtained by combining the phonon contributions computed at the lower level of theory with electronic cohesive energies computed via the higher-level single point energies as $A(T,V) = E_{coh}(V) + A_{vib}(T,V)$. This enables expression of any relevant thermodynamic property at finite temperatures and pressures (e.g. density or isobaric heat capacity) via the fundamental thermodynamic relationships. Standard sublimation enthalpies at 0 K were computed according to the equation:

$$\Delta_{\mathrm{sub}}H^{0} = E_{\mathrm{el}}^{\mathrm{mol}} - E_{\mathrm{el}}^{\mathrm{cr}}(V_0) + \Delta_{\mathrm{ZP}}E(V_0), \quad (1)$$

where $E_{\mathrm{el}}^{\mathrm{cr}}$ is the unit-cell electronic energy valid for the equilibrium quasi-harmonic unit-cell volume V_0 at 0 K , electronic energies of isolated molecules $E_{\mathrm{el}}^{\mathrm{mol}}$ (in optimized gas-phase geometry), and the difference of zero-point vibrational energies of the vapor and crystalline phases $\Delta_{\mathrm{ZP}}E(V_0)$. Standard sublimation entropies were computed according to the equation:

$$\Delta_{\mathrm{sub}}S^{0} = S^{\mathrm{g0}} - S^{\mathrm{cr}}, \quad (2)$$

being the difference of the absolute entropy of ideal gas S^{g0} at the standard pressure (100 kPa) and the entropy of a crystal S^{cr} in accordance with the third law of thermodynamics. Sublimation enthalpies and entropies were temperature-adjusted using the isobaric heat capacities of both phases. Finally, the sublimation pressure at each temperature was computed by solving for the pressure at which the Gibbs energy of sublimation is zero.

Reference experimental data was derived using the previously described procedure,[41] evaluating the sublimation enthalpy on the basis of the literature data on saturated sublimation (or vaporization if necessary) pressures (available for ethane,[76, 77] methanol,[78, 79] benzene,[80] imidazole[81-83]). For ethane, where only the vaporization enthalpy is obtained in this way, the enthalpy of fusion needs to be added to evaluate the enthalpy of sublimation at the at the triple-point temperature.[84, 85] Experimental sublimation entropy was obtained from the experimental isobaric heat capacities for the crystal covering the temperature range from 0 K to the triple-point temperature (for ethane,[84] methanol,[78] benzene,[86] and imidazole[81]), and from the isobaric heat capacity of the ideal gas computed from the experimental vibrational frequencies and other spectral data (for ethane,[87, 88] methanol,[89, 90] benzene,[80] and imidazole[91]) using the RRHO model with optional 1D-HR corrections in case of ethane and methanol. The given heat capacities were also used for temperature-adjustments of experimental sublimation enthalpies, entropies and pressures. Calculated Γ-point vibrational frequencies were compared

with the available experimental data (for ethane,[92, 93] methanol,[94, 95] benzene,[96-98] and imidazole[99-101]). See our previous work for the same analysis performed for methanol.[32]

3. RESULTS AND DISCUSSION

The performance of various computational levels of theory for calculation of p_{sub} is discussed here, taking into account the accuracy of both the calculated standard $\Delta_{sub}H$ and $\Delta_{sub}S$ contributions to p_{sub}. Section 3.1 first examines how different electronic structure models used for the 1- and 2-body calculations perform using Amoeba for the long-range and many-body contributions and DFT geometries and phonons. Section 3.2 then assesses the importance of the many-body treatment and the possibility of refining the geometries at the fragment-based MP2 level of theory.

TABLE 2
Comparison of p_{sub} (Pa) calculated at various levels of theory with the experimental values, relevant for the temperatures T_{pt} (K) of the lowest-lying phase transition.

	Ethane	Methanol	Benzene	Imidazole
T_{pt}	89.73	157.34	278.674	362.25
p_{sub}^{exp}	$(1.11\pm0.10)\cdot10^{0}$	$(5.50\pm1.10)\cdot10^{-3}$	$(4.79\pm0.01)\cdot10^{3}$	$(1.05\pm0.05)\cdot10^{2}$
MP2/avtz+Amoeba@DFT[a]	$1.02\cdot10^{2}$	$8.13\cdot10^{-1}$	$2.11\cdot10^{1}$	$2.00\cdot10^{0}$
MP2/cbs+Amoeba@DFT[a]	$3.57\cdot10^{1}$	$9.48\cdot10^{-2}$	$5.84\cdot10^{0}$	$3.98\cdot10^{-1}$
CCSD(T)/cbs+Amoeba@DFT[a]	$7.81\cdot10^{0}$	$9.76\cdot10^{-2}$	$1.56\cdot10^{3}$	$2.70\cdot10^{1}$
MP2C-F12/avdz+Amoeba@DFT[a]	$1.21\cdot10^{1}$	$1.08\cdot10^{-1}$	$2.30\cdot10^{3}$	$1.26\cdot10^{1}$
DW-CCSD(T)-F12/avdz+Amoeba@DFT[a]	$1.64\cdot10^{1}$	$1.11\cdot10^{-1}$	$1.39\cdot10^{3}$	$2.50\cdot10^{1}$
CCSD(T)/cbs+pHF@DFT[a]	$2.85\cdot10^{1}$	$1.37\cdot10^{-1}$	$1.07\cdot10^{4}$	$8.17\cdot10^{1}$
MP2D-F12/avdz+Amoeba@DFT[a]	-	-	$1.83\cdot10^{3}$	$1.31\cdot10^{1}$

CCSD(T)/cbs+Amoeba@MP2[b]	$5.51 \cdot 10^{-2}$	$3.25 \cdot 10^{-3}$	-	-
CCSD(T)/cbs+pHF@MP2[b]	$2.60 \cdot 10^{-1}$	$2.08 \cdot 10^{-2}$	-	-

[a] Unit-cell geometries optimized at the PBE-D3(BJ)/PAW level in VASP.
[b] Unit-cell geometries optimized at the MP2/aug-cc-pVTZ + Amoeba in HMBI.

3.1 Dependence on the choice of QM model

Figure 2 presents the results obtained for ethane using DFT-based geometries with *ab-initio*-refined E_{coh} (including Amoeba many-body contributions). The calculated $\Delta_{sub}H$ and $\Delta_{sub}S$ exhibit systematic improvement as one moves to increasingly accurate *ab initio* approaches. The temperature trends of both properties are well-captured by all levels of theory, indicating reliable heat capacity calculations for both gas and crystalline phases. However, both sublimation enthalpy and entropy are considerably underestimated (e.g. for CCSD(T)/cbs + Amoeba, $\Delta_{sub}H$ by 3 kJ·mol^{-1} ≈ 15 % and $\Delta_{sub}S$ by 20 J·K^{-1}·mol^{-1} ≈ 15 %) which is probably due to the massive distortion of the DFT unit-cell geometry compared to experiment, see Tables 1 and S1. Most notably, the *b* lattice constant is overestimated by 1.6 Å, while the β angle is underestimated by 20º.

Although the fact that both $\Delta_{sub}H$ and $\Delta_{sub}S$ are underestimated leads to some fortuitous error cancellation, the large errors in $\Delta_{sub}H$ and $\Delta_{sub}S$ translate to overestimation of the CCSD(T)/CBS+Amoeba p_{sub} curve by 1-4 orders of magnitude compared to experiment. The massive overestimation of p_{sub} for ethane at low temperatures decreases somewhat with increasing temperature because the underestimated $\Delta_{sub}H$ also translates to a smaller slope of the temperature-dependence of p_{sub}. For this reason, the error of computed p_{sub} is strongly temperature dependent, and better agreement between theory and experiment is achieved at higher temperatures for all methods. See Table 2 for individual values.

FIGURE 2. Standard sublimation enthalpies (left), standard sublimation entropies (middle), and error of calculated sublimation pressures (right) for ethane, calculated based on DFT-

based geometries and HMBI single-point ab initio refinements of E_{coh} including Amoeba embedding.

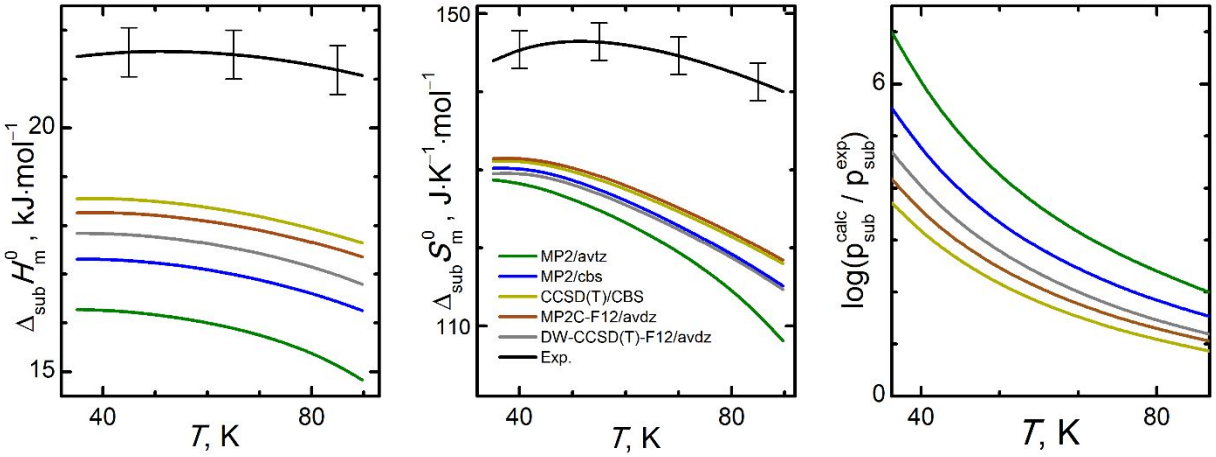

The situation for methanol is somewhat different, as illustrated in Figure 3. The calculated CCSD(T)/cbs + Amoeba p_{sub} are overestimated by 1-2 orders of magnitude, and most of the other methods yield very similar results. No systematic improvement is observed along the nominally improving hierarchy of *ab initio* theories. The notable outlier is MP2/aug-cc-pVTZ, which exhibits an error in $\Delta_{sub}H$ that is twice as large as those in the complete-basis-set methods, highlighting the importance of using large basis sets. More specifically, the gold-standard CCSD(T)/cbs + Amoeba $\Delta_{sub}H$ values are underestimated roughly by 3 kJ·mol^{-1} ≈ 5 %, but $\Delta_{sub}S$ is overestimated by 12 J·K^{-1}·mol^{-1} ≈ 8 %). The opposite signs of these two errors means that the errors combine for p_{sub} of methanol, in contrast to the error cancellation observed in the ethane case above. Furthermore, the enthalpic error dominates over the entropic one, which can be seen in how the errors in p_{sub} decrease with temperature. This is partly due to the magnitude of the error of $\Delta_{sub}H$ and partly to the fact that the entropic $T\,\Delta_{sub}S$ term is less significant at the given lower temperatures.

Although the 1-body and 2-body *ab initio* interaction energies should provide relatively high accuracy for methanol, the long-range and many-body Amoeba treatment may not be quite as good and could account for the observed lack of systematic improvement. In our earlier study on the methanol phase diagram, Amoeba overestimated the polarization energy in the alpha crystalline phase appreciably.[31, 32] Furthermore, we note here that above 70 K, the

experimental $\Delta_{sub}H$ and $\Delta_{sub}S$ both decrease with temperature, since $C_p^{cr} > C_p^{g0}$ under those conditions. The theoretical models do not reproduce this temperature dependence properly, since they incorrectly predict that $C_p^{cr} > C_p^{g0}$ occurs only above 145 K. This means that the calculated C_p^{cr} and related thermal expansivity of methanol are underestimated appreciably (see Figure S4), which also agrees with our earlier α methanol modeling results, indicating that HMBI MP2/avtz+Amoeba phonons are superior to the PBE-D3(BJ) counterparts.[31, 32] Mean absolute percentage deviations for the Γ-point frequencies of the lattice modes are 15% and 19% and of the intramolecular modes 2.4% and 3.3%, for MP2/avtz+Amoeba and PBE-D3(BJ) methods respectively (see Figure S3).[31]

FIGURE 3. Standard sublimation enthalpies (left), standard sublimation entropies (middle), and error of calculated sublimation pressures (right) for methanol, calculated based on DFT-based geometries and HMBI single-point *ab initio* refinements of E_{coh} (with Amoeba many-body contributions).

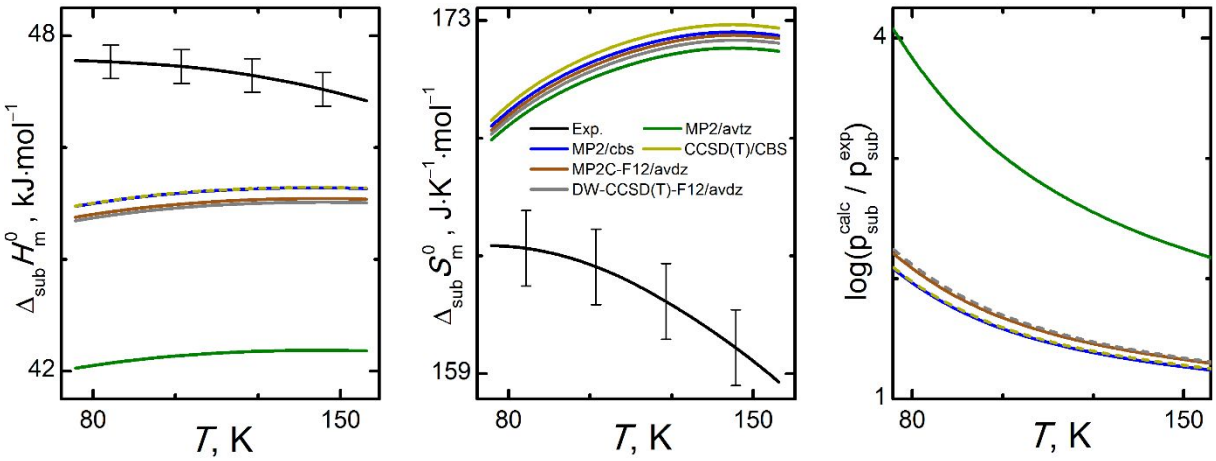

Figures 4 and 5 illustrate the calculated sublimation properties for benzene and imidazole, respectively. Relatively similar conclusions can be drawn for both crystals. The temperature trends of $\Delta_{sub}H$ and $\Delta_{sub}S$ are well-captured by the calculations. Mean absolute percentage deviations of the Γ-point frequencies of the lattice modes are 9.0% and 6.0% and of the intramolecular modes 1.1% and 2.1%, for crystalline benzene and imidazole respectively (see Figures S5 and S7). It is no surprise that small basis set MP2 calculations strongly overbind

the cohesion of aromatic molecules, due to both basis set incompleteness/superposition error and the well-known problems MP2 has in overestimating dispersion interactions.[102] These issues translate to several orders of magnitude error in the MP2/aug-cc-pVTZ p_{sub} for both species. The quality of the predictions is appreciably improved when higher level *ab initio* methods are employed. Namely, the gold-standard CCSD(T)/cbs + Amoeba and silver-standard DW-CCSD(T)-F12/aug-cc-pVTZ + Amoeba approximations yield almost identical results for all sublimation properties (for benzene overestimation of $\Delta_{sub}H$ by 4 kJ·mol^{-1} ≈ 9 % and $\Delta_{sub}S$ by 7 J·K^{-1}·mol^{-1} ≈ 5 %, and for imidazole overestimation of $\Delta_{sub}H$ by 2 kJ·mol^{-1} ≈ 2 % and $\Delta_{sub}S$ by 1 J·K^{-1}·mol^{-1} ≈ 1 %). The results of the bronze standard MP2C-F12/aug-cc-pVDZ + Amoeba approximation also lie very close. In fact, both dispersion-corrected MP2 approaches used in this work, namely MP2C-F12 and MP2D-F12, coupled with the aug-cc-pVDZ basis set, yield almost identical results of all three sublimation properties in these two crystals. This provides additional evidence that the MP2D method represents a viable tool for obtaining accurate interaction energies, taking into account that it is appreciably more straightforward to compute MP2D energies compared to their MP2C counterparts and that MP2D possesses analytical gradients.[72] For both crystals, the relatively small errors in $\Delta_{sub}H$ and $\Delta_{sub}S$ and the effective error cancellation translate to small p_{sub} errors that lie within a single order of magnitude or so from experiment. Such an achievement should be regarded as successful and relatively reliable prediction of p_{sub} from first principles. Notably, better results were obtained for polar hydrogen-bonded imidazole which exhibits the highest cohesive energy among the four studied crystals.

FIGURE 4. Standard sublimation enthalpies (left), standard sublimation entropies (middle), and error of calculated sublimation pressures (right) for benzene, calculated based on DFT-based geometries and HMBI single-point ab initio refinements of E_{coh} including Amoeba many-body contributions.

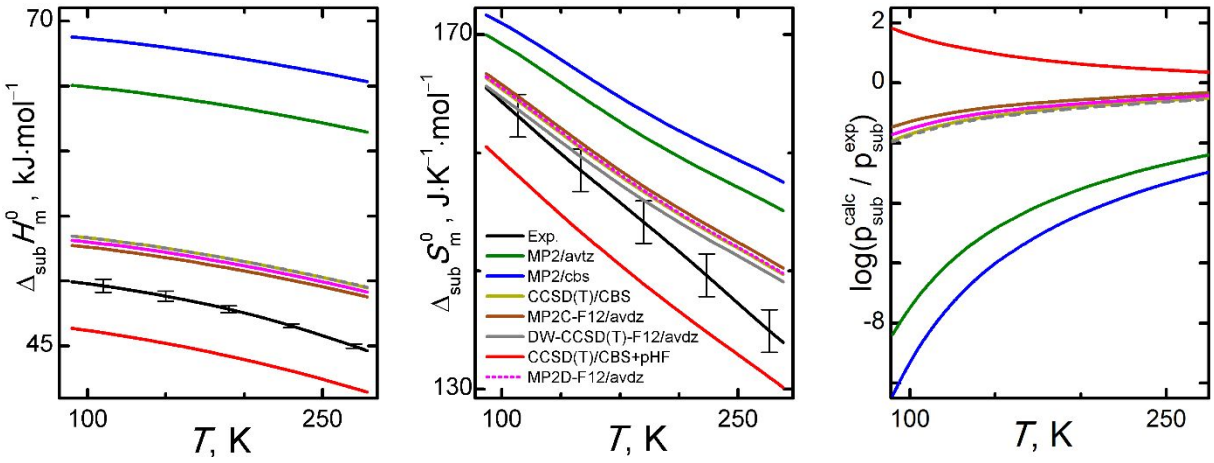

For most of the methods, the errors in the predicted $\Delta_{sub}H$ and $\Delta_{sub}S$ for benzene and imidazole possess the opposite sign compared to those in ethane. When combined, the predicted p_{sub} is strongly underestimated at low temperatures, but the errors decrease with increasing temperature because the overestimated $\Delta_{sub}H$ translates to a larger slope of p_{sub}.

FIGURE 5. Standard sublimation enthalpies (left), standard sublimation entropies (middle), and error of calculated sublimation pressures (right) for imidazole, calculated based on DFT-based geometries and HMBI single-point ab initio refinements of E_{coh} including Amoeba many-body contributions.

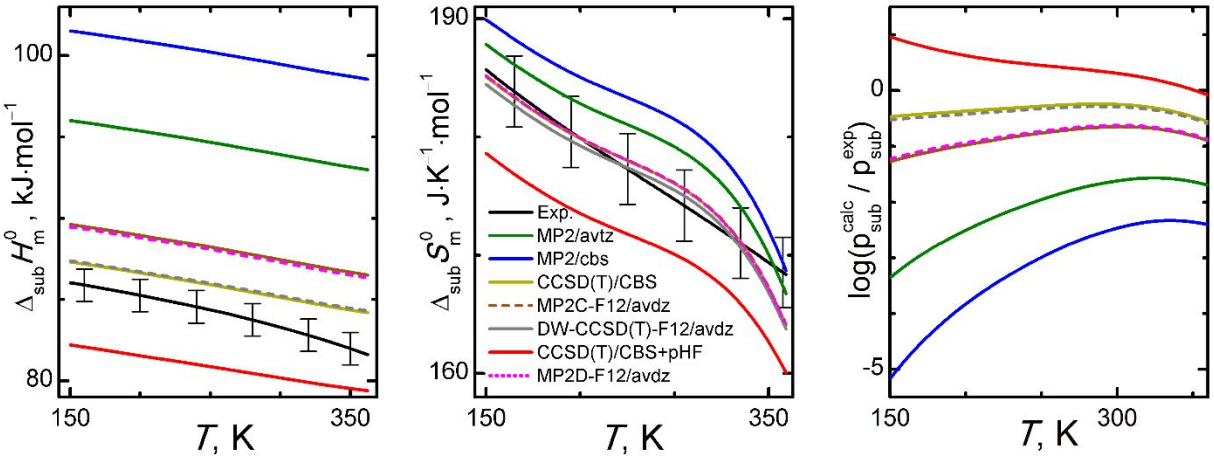

3.2 Investigation of the many-body treatment and of the quality of unit-cell geometries

To investigate the appropriateness of using the classical Amoeba force field for treating the long-range and many-body interactions in the HMBI model, calculations of those contributions were also performed at the periodic Hartree-Fock level of theory. Figures 6 and 7 compile results obtained for ethane and methanol, respectively, at the CCSD(T)/CBS+pHF and CCSD(T)/CBS+Amoeba levels for both DFT-based and MP2-based geometries.

FIGURE 6. Comparison of the results obtained for ethane, combining CCSD(T)/CBS treatment of the short-range dimers with Amoeba or pHF many-body treatments. Results were obtained using either DFT or MP2-optimized unit-cell geometries and phonons, or optionally with experimental vibrational frequencies (XF data set) or with both experimental vibrational frequencies and thermal expansion (XFE data set).

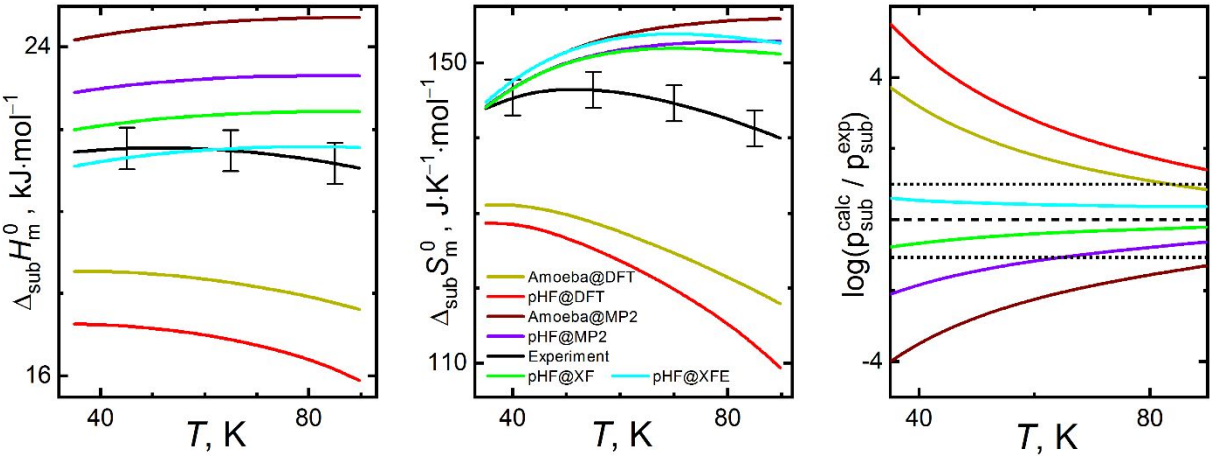

As described above, the DFT-based crystalline ethane geometry significantly distorted the β unit cell angle (by 20º) and overestimated the b lattice constant by 1.6 Å. Optimizing the geometries at the MP2/aug-cc-pVDZ + Amoeba level instead produces a unit cell in much better agreement with experiment (Table 1), with errors of only ~0.1 Å (2-3%) in the lattice constants and 0.8º in the β angle. Whereas the CCSD(T)/cbs calculations on the DFT geometries underestimated $\Delta_{sub}H$ of ethane, the same single-point energy calculations on the MP2 geometries overestimate $\Delta_{sub}H$ by a comparable amount.

Replacing the Amoeba many-body terms with pHF-based ones decreases $\Delta_{sub}H$, for both the MP2 and DFT geometries. However, the best agreement with the experimental $\Delta_{sub}H$ (within 1-2 kJ·mol^{-1}) comes from the combination of MP2 geometries and pHF-based many-body contributions. On the other hand, using the MP2 geometries (and phonons) produces incorrect temperature trends for both $\Delta_{sub}H$ and $\Delta_{sub}S$, unlike for the DFT-based geometries. This plays, however, only a minor role in the accuracy of the resulting p_{sub}. For the CCSD(T)/CBS+pHF single point calculations on the MP2 geometries, error compensation resulting from

overestimation of both $\Delta_{sub}H$ and $\Delta_{sub}S$ translates to the predicted p_{sub} differing from the experiment only by a factor of four at the triple point temperature.

FIGURE 7. Comparison of the results obtained for methanol, combining CCSD(T)/CBS treatment of the proximate pairs gradually with DFT-based or MP2-based unit-cell geometries and phonons and with Amoeba or pHF embedding, or optionally with experimental vibrational frequencies (XF data set) or with both experimental vibrational frequencies and thermal expansion (XFE data set).

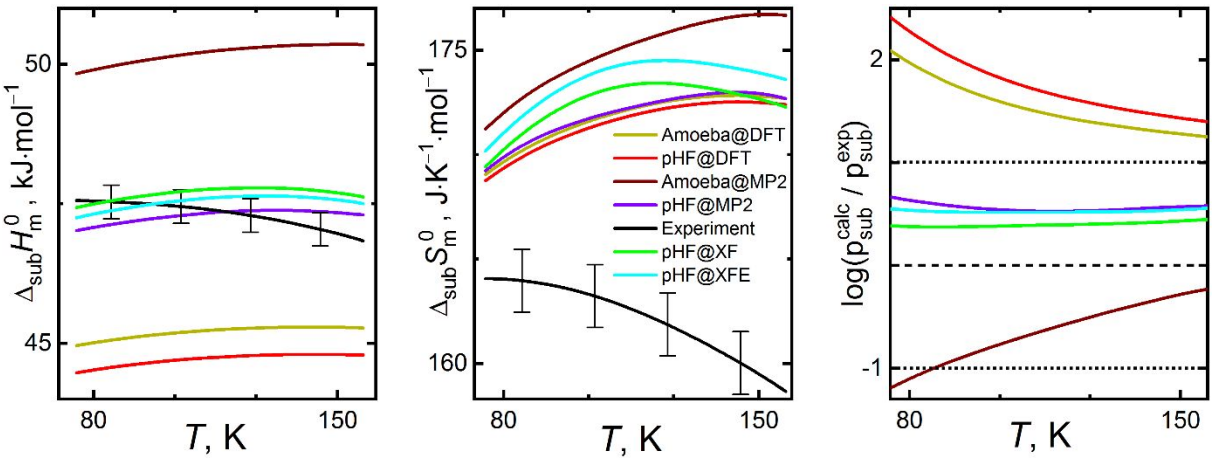

Next, we consider the same dependence of the predicted properties on geometry and many-body treatment for methanol.

Figure 7 confirms what has already been demonstrated in our previous works on polymorphism of methanol:[31, 32] Methanol exhibits strong cooperative hydrogen bonding effects that are better described via periodic HF than Amoeba. Adopting the pHF description of the many-body contributions improves the accuracy of the calculated $\Delta_{sub}H$, especially when coupled with the HMBI MP2-based geometries which seem to be superior to the DFT-based ones. Using the CCSD(T)/CBS+pHF level of theory for refinement of E_{coh} for MP2-based geometries leads to highly accurate $\Delta_{sub}H$ predictions that match experiment with a sub-kJ·mol^{-1} accuracy over a broad temperature range. On the other hand, such an improvement was not observed for predicted $\Delta_{sub}S$. The entropies are much less sensitive to the quality of the underlying unit-cell geometries or many-body treatment. $\Delta_{sub}S$ is influenced by these factors only indirectly through the steepness of the $E_{coh}(V)$ wells, which affects the thermal

expansivity and isobaric heat capacity trends. Altogether, highly accurate $\Delta_{sub}H$ and moderately accurate $\Delta_{sub}S$ yield p_{sub} differing from experiment only by a factor of 4 or better over a broad temperature range, see the purple lines in Figure 7.

When the *ab initio* data on the molar Gibbs energy of the crystalline β-phase of methanol from our previous work[32] are combined with the results obtained in this work for the α-polymorph and vapor, the coordinates of the respective triple point (α-β-vapor) can be computed. At the CCSD(T)/CBS+pHF level of theory (incorporating MP2 geometries and phonons), the molar Gibbs energies of all three phases are equal at 80.55 K and at $2.2 \cdot 10^{-17}$ Pa, versus 157.34 K and $5.5 \cdot 10^{-3}$ Pa experimentally.[78, 79] The agreement of calculated and experimental temperatures are still reasonable and such a 77 K difference corresponds to a mere 0.4 kJ·mol^{-1} uncertainty of Gibbs energy.[32] On the other hand, the massive disagreement for the predicted triple-point pressure may seem fatal at the first sight. Such a result, nevertheless, only corresponds to the change of p_{sub} from the 77 K temperature error. If the CCSD(T)/CBS+pHF-based p_{sub} is evaluated at the experimental triple-point temperature, one obtains a reasonable value of $2.1 \cdot 10^{-2}$ Pa, which differs by only a factor of 4 from experiment. To conclude, this illustrates how predicting the temperature – pressure coordinates of a triple point where one of the phases in equilibrium is the vapor is probably the most difficult task in the field of *ab initio* calculations of phase equilibria and polymorphism.

For CCSD(T) calculations for both benzene and imidazole, replacing the Amoeba many-body contributions with the pHF counterparts yields appreciable underestimation of their $\Delta_{sub}H$ and $\Delta_{sub}S$, see Figures 4 and 5. The many-body contributions to $\Delta_{sub}H$ and $\Delta_{sub}S$ obtained from pHF are 7 and 5 kJ·mol^{-1} lower and 12 and 6 J·K^{-1}·mol^{-1} lower compared to the Amoeba results for benzene and imidazole, respectively. The differences in entropies arise as pHF yields steeper $E(V)$ wells than Amoeba which translates into lower pHF heat capacities and entropies of the crystal. As replacing Amoeba with pHF many-body terms only changes the sign of the errors of both $\Delta_{sub}H$ and $\Delta_{sub}S$, not decreasing the error magnitude, the resulting

CCSD(T)/cbs + pHF p_{sub} are overestimated (up to 2 orders of magnitude at lower temperatures, roughly by a factor of 2 at the temperature of the triple point). Note that the most significant improvement of the results thanks to the pHF many-body contributions was observed for ethane and methanol in combination with MP2 geometries and phonons. However, MP2 geometries and phonon calculations were not performed for benzene and imidazole in this work due to computational expense.

3.3 Investigation of the quality of phonon calculations

Mean absolute percentage errors of the Γ-point frequencies of the lattice modes of ethane and methanol are given in Table 3, see Figures S1 and S3 for a graphical representation. Frequencies of the intramolecular (internal) modes calculated using either MP2/aug-cc-pVDZ + Amoeba or PBE-D3(BJ)/PAW methods differ no more than by 2.5% on average (PBE-D3 data set is more accurate relative to experiment for the internal modes here). The experimental modes were predominantly measured at 20 K for both ethane and methanol.[92-95] The level of agreement between the theoretical and experimental internal mode frequencies varies only slightly (by a few tenths of a percentage point on average) depending on whether the comparison is performed based on predicted frequencies obtained as: i) the Γ-point frequencies computed for the optimized unit-cell given by the minimum electronic energy, or ii) the quasi-harmonic frequencies interpolated using the Grüneisen parameters to the quasi-harmonic unit-cell volume at 20 K, or iii) the quasi-harmonic frequencies interpolated using the Grüneisen parameters to the experimental unit-cell volumes at 20 K. Qualitatively similar behavior was found in our earlier work. [31]

On the other hand, MP2/aug-cc-pVDZ + Amoeba frequencies are more accurate than the PBE-D3 ones for the lattice modes of both ethane and methanol. Furthermore, the choice of the three aforementioned schemes for predicting the 20 K frequencies affects the error statistics considerably, especially for the lowest-frequency lattice modes, see Figures S1 and S3.

TABLE 3
Mean absolute percentage errors of the calculated Γ-point frequencies of the lattice modes of ethane and methanol, evaluated either for the unit-cell volumes corresponding to the predicted minimum of the electronic energy (V_{EL}), or for frequencies interpolated using the Grüneisen parameters for the quasi-harmonic volumes at the temperature of experimental determination (V_{QHA}) and experimental volumes at 20 K (V_{EXP}).

Crystal	Data set	V_{EL}	V_{QHA}	V_{EXP}	V_{EL}	V_{QHA}	V_{EXP}
		HMBI MP2/avtz+Amoeba			PBE-D3(BJ)/PAW		
Ethane	Lattice modes	10.9%	11.6%	8.7%	18.0%	30.2%	18.7%
	Internal modes	3.9%	3.8%	3.8%	1.7%	1.6%	1.7%
Methanol	Lattice modes	11.5%	11.8%	11.3%	16.0%	18.4%	16.5%
	Internal modes	5.8%	5.7%	5.7%	4.6%	4.7%	4.6%

Now consider the impact of these errors in the frequencies on the predicted crystal structures and properties. For ethane, most of the MP2/aug-cc-pVDZ + Amoeba phonon frequencies (V_{EL} data set) of the lattice modes are overestimated, which translates to underestimation of the unit cell volumes and heat capacities predicted at this level of theory. In contrast, their PBE-D3(BJ)/PAW counterparts are underestimated (see Figure S1), resulting in overestimation of the volumes and heat capacities for ethane. The oppositely signed errors in the predicted phonon frequencies obtained at both levels can be observed also in the different slopes of respective $\Delta_{sub}S$ curves in Figure 6.

In case of methanol, MP2/avtz+Amoeba and PBE-D3(BJ) phonons (meaning that also molar volumes and heat capacities) do not differ as much as they do for ethane. MP2 yields somewhat lower frequencies than PBE-D3(BJ) for the lowest-lying lattice modes (getting

excited at the lowest temperatures), see Figure S3. This behavior translates to slightly different trends of the heat capacities of crystalline methanol (given in Figure S4) which are, however, not that significant to affect the trends of $\Delta_{sub}S$.

To investigate the role of the phonon accuracy in the thermochemical predictions further, we consider the possibility of replacing the predicted phonon frequencies with their experimental values. Although a complete experimental assignment of frequencies of the lattice modes is not available for neither for ethane nor methanol, the few missing frequency values can be tentatively added assuming frequency degeneracies and resulting peak overlaps in the respective spectra. Plugging such experimental phonon frequencies and experimental frequencies for the vapor phase to our quasi-harmonic calculations (still retaining the ab initio-computed Grüneisen parameters) at the CCSD(T)/CBS+pHF level resulted in new data sets (labelled XF) of sublimation properties for ethane and methanol in Figures 6 and 7, respectively. Going one step further, the steepness and the position of the minimum in the $E_{coh}(V)$ wells were adjusted to best reproduce the experimental thermal expansivity trends of the crystals. This procedure resulted in another data set (labelled XFE) of sublimation properties.

Both experimentally-based refinements improve the accuracy of $\Delta_{sub}H$ non-negligibly. The respective $\Delta_{sub}H(T)$ curves in Figures 6 and 7 exhibit nearly identical curvature, albeit with different vertical offsets. This indicates that the differences between the XF and XFE occur mainly due to changes in the zero point vibrational contribution to $\Delta_{sub}H$. Especially for ethane, an agreement of experimental and XFE $\Delta_{sub}H$ well within the experimental uncertainty is reached over a broad temperature interval. As a consequence, resulting XF and XFE data sets reproduce the experimental p_{sub} values to within factor of 3 or better. This slight temperature dependence of the p_{sub} error arises from the small errors in $\Delta_{sub}H$ (i.e. it impacts the slope of $p_{sub}(T)$), while the remaining vertical offset factor is primarily due to the remaining error seen in both XF and XFE $\Delta_{sub}S$ data sets. Using experimental vibrational

frequencies and correcting for the experimental thermal expansivity in the given quasi-harmonic computational model fails to correct strongly underestimated isobaric heat capacities of the crystals of ethane and methanol fully. Uncertainties in the experimental frequencies and factors such as strong anharmonicity or phonon dispersion, not accounted for in the XF and XFE data sets, might contribute to this behavior. There is not enough experimental data for crystalline benzene and imidazole to perform analogous analyses of phonon-related uncertainty for these species.

Overall, these results suggest that while the predicted quasi-harmonic phonon frequencies are fairly good, the remaining uncertainties do significantly impact the predicted thermochemistry and sublimation pressures. Errors in the curvature and minima of the electronic energy wells appear to have a smaller impact on the results. Further reduction in the computational uncertainties could be achieved by using purely experimental input data on $\Delta_{sub}H$ and $\Delta_{sub}S$, an approach essentially equivalent to that used in our previous work, denoted Tier Y p_{sub} data set, [41] the uncertainty of which was evaluated to 68%.

5. CONCLUSIONS

We presented a thorough comparison of performance of several ab initio approaches to calculations of sublimation pressures for four molecular crystals. Given the extreme sensitivity of p_{sub}, contemporarily affordable quantum chemical methods are not likely to predict p_{sub} with a higher accuracy than a factor of 2-10 on a routine basis. Still, such a computational uncertainty makes the state-of-the-art *ab initio* p_{sub} more reliable than the results of some semi-empirical estimative approaches and possibly as accurate as experimental determinations in the extreme sub-Pascal region. In this context, the question posed in the title of this work can be answered in a way that *ab initio* p_{sub} for molecular crystals can be considered as fairly reliable for small to medium-size molecules and unit cells (enabling to use high-level correlated wavefunction theories) although the overall

computational uncertainty hardly reaches the level accessible for enthalpic properties. The calculations presented here indicate that it is possible to converge the standard sublimation enthalpy to within 1-2 kJ·mol^{-1} and the standard sublimation entropy to within 5 J·K^{-1}·mol^{-1}. When the errors in $\Delta_{sub}H$ and $\Delta_{sub}S$ possess the same sign, additional error compensation that improves the quality of the predicted sublimation pressure can occur. This manifests as a strong temperature dependence in the error of the predicted p_{sub}, with the magnitude of the error decreasing appreciably at higher temperatures. Taken together, these results indicate that p_{sub} should be expected to exhibit orders-of-magnitude errors unless the underlying predicted $\Delta_{sub}H$ is converged to the sub-kJ·mol^{-1} level. With the typical errors that occur for current quasi-harmonic phonon calculations, the errors in p_{sub} can increase up to ten-fold.

Because the high-level *ab initio* single-point energy refinements were performed using unit-cell geometries optimized at lower levels of theory, the quality of the underlying geometries and their compatibility with the higher level of theory becomes an important factor in determining the overall accuracy. For both ethane and methanol, optimized unit-cell geometries and the lattice-mode phonons calculated using HMBI at the MP2/aug-cc-pVTZ+Amoeba level are superior to the PBE-D3(BJ)/PAW counterparts while the related geometry-related energy difference amounts to units of kJ·mol^{-1}. Periodic Hartree-Fock treatment of the many-body terms in HMBI yielded less bound crystals than Amoeba did for all four crystals investigated. Coupled with DFT geometries, pHF usually did not bring significant improvement of $\Delta_{sub}H$ which is in contrast with the results obtained for MP2 geometries, for which CCSD(T)+pHF always yielded p_{sub} in the closest agreement with experiment. Finally, it was demonstrated that replacing the predicted phonon frequencies with experimental ones leads to even better agreement in the sublimation enthapies and pressures. This highlights how, despite the seemingly reasonable agreement between theory and experimental phonon frequencies found here, obtaining truly quantitative accuracy will require even more accurate phonon treatments.

ASSOCIATED CONTENT

Supporting Information

The supporting information is available free of charge on the ACS Publications website at DOI:

1. Calculated equilibrium unit-cell volumes.
2. Comparison of calculated and experimental phonon frequencies.
3. Calculated isobaric heat capacities of the crystals and vapor.

AUTHOR INFORMATION

Corresponding Author

* E-mail: cervinkc@vscht.cz

ACKNOWLEDGMENT

C. Č acknowledges financial support from the The Ministry of Education, Youth and Sports of the Czech Republic from the Project No. LTAUSA18011, being a part of the INTER-EXCELLENCE program, and the access to computing facilities under the program the Large Infrastructures for Research, Experimental Development and Innovations project „IT4Innovations National Supercomputing Center – LM2015070“. G.B. acknowledges financial support from the United States National Science Foundation (CHE-1665212) and computing resources from XSEDE (TG-CHE110064).

REFERENCES

1. A. Delle Site, *J. Phys. Chem. Ref. Data*, 1997, **26**, 157-193.
2. K. Růžička, M. Fulem and V. Růžička, *J. Chem. Eng. Data*, 2005, **50**, 1956-1970.
3. K. Růžička and V. Majer, *J. Phys. Chem. Ref. Data*, 1994, **23**, 1-39.
4. K. Růžička and V. Majer, *AIChE J.*, 1996, **42**, 1723-1740.
5. Y.-C. Su, Y. A. Liu, C. A. Diaz Tovar and R. Gani, *Ind. Eng. Chem. Res.*, 2011, **50**, 6809-6836.
6. Z. Kolská, J. Kukal, M. Zábranský and V. Růžička, *Ind. Eng. Chem. Res.*, 2008, **47**, 2075-2085.
7. F. S. Emami, A. Vahid, J. R. Elliott and F. Feyzi, *Ind. Eng. Chem. Res.*, 2008, **47**, 8401-8411.
8. J. F. Pankow and W. E. Asher, *Atmos. Chem. Phys.*, 2008, **8**, 2773-2796.

9. M. Staikova, F. Wania and D. J. Donaldson, *Atmospheric Environ.*, 2004, **38**, 213-225.
10. D. Ambrose and N. C. Patel, *J. Chem. Thermodyn.*, 1984, **16**, 459-468.
11. D. Ambrose and J. Walton, *Pure Appl. Chem.*, 1989, **61**, 1395-1403.
12. C. Červinka, M. Fulem and K. Růžička, *J. Chem. Eng. Data*, 2012, **57**, 227-232.
13. C. Červinka, M. Fulem and K. Růžička, *J. Chem. Eng. Data*, 2013, **58**, 1382-1390.
14. C. Červinka, M. Fulem, V. Štejfa and K. Růžička, *J. Chem. Eng. Data*, 2017.
15. G. J. O. Beran and K. Nanda, *J. Phys. Chem. Lett.*, 2010, **1**, 3480.
16. P. J. Bygrave, N. L. Allan and F. R. Manby, *J. Chem. Phys.*, 2012, **137**, 164102.
17. C. Červinka, M. Fulem and K. Růžička, *J. Chem. Phys.*, 2016, **144**, 064505.
18. J. C. Sancho-Garcia, J. Arago, E. Orti and Y. Olivier, *J. Chem. Phys.*, 2013, **138**, 204304.
19. O. Sode and S. Hirata, *J. Phys. Chem. A*, 2010, **114**, 8873-8877.
20. K. Nagayoshi, K. Kitaura, S. Koseki, S. Y. Re, K. Kobayashi, Y. K. Choe and S. Nagase, *Chem. Phys. Lett.*, 2003, **369**, 597-604.
21. D. J. Carter and A. L. Rohl, *J. Chem. Theory Comput.*, 2014, **10**, 3423-3437.
22. B. Civalleri, K. Doll and C. M. Zicovich-Wilson, *J. Phys. Chem. B*, 2007, **111**, 26.
23. S. Grimme, J. Antony, S. Ehrlich and H. Krieg, *J. Chem. Phys.*, 2010, **132**, 154104.
24. K. Lee, E. D. Murray, L. Kong, B. I. Lundqvist and D. C. Langreth, *Phys. Rev. B*, 2010, **82**, 081101.
25. L. Maschio, D. Usvyat, M. Schuetz and B. Civalleri, *J. Chem. Phys.*, 2010, **132**, 134706.
26. J. Moellmann and S. Grimme, *J. Phys. Chem. C*, 2014, **118**, 7615-7621.
27. C. Muller, D. Usvyat and H. Stoll, *Phys. Rev. B*, 2011, **83**, 245136.
28. J. Klimeš, *J. Chem. Phys.*, 2016, **145**.
29. S. Hirata, K. Gilliard, X. He, J. Li and O. Sode, *Acc. Chem. Res.*, 2014, **47**, 2721.
30. J. Yang, W. F. Hu, D. Usvyat, D. Matthews, M. Schutz and G. K. L. Chan, *Science*, 2014, **345**, 640.
31. C. Červinka and G. J. O. Beran, *Phys. Chem. Chem. Phys.*, 2017, **19**, 29940-29953.
32. C. Červinka and G. J. O. Beran, *Chem. Sci.*, 2018, **9**, 4622-4629.
33. C. Červinka, M. Fulem, R. P. Stoffel and R. Dronskowski, *J. Phys. Chem. A*, 2016, **120**, 2022-2034.
34. R. P. Stoffel, C. Wessel, M.-W. Lumey and R. Dronskowski, *Angew. Chem. Int. Edit.*, 2010, **49**, 5242.
35. J. G. Brandenburg, J. Potticary, H. A. Sparkes, S. L. Price and S. R. Hall, *J. Phys. Chem. Lett.*, 2017, **8**, 4319-4324.
36. J. George, R. M. Wang, U. Englert and R. Dronskowski, *J. Chem. Phys.*, 2017, **147**.
37. V. L. Deringer, J. George, R. Dronskowski and U. Englert, *Acc. Chem. Res.*, 2017, **50**, 1231-1239.
38. J. L. McKinley and G. J. O. Beran, *Faraday Discuss.*, 2018, **211**, 181-207.
39. Y. N. Heit and G. J. O. Beran, *Acta Crystallogr. B*, 2016, **72**, 514-529.
40. Y. N. Heit, K. D. Nanda and G. J. O. Beran, *Chem. Sci.*, 2015, DOI: 10.1039/C5SC03014E, In Press.
41. C. Červinka and M. Fulem, *Cryst. Growth Des.*, 2019, **19**, 808-820.
42. J. Hoja, A. M. Reilly and A. Tkatchenko, *Wiley Interdiscip. Rev. Comput. Mol. Sci.*, 2017, **7**, e1294.
43. S. Hirata, *Mol. Phys.*, 2010, **108**, 3113-3124.
44. B. Monserrat, N. D. Drummond and R. J. Needs, *Phys. Rev. B*, 2013, **87**, 144302.
45. M. T. Ruggiero, J. A. Zeitler and A. Erba, *Chem. Commun.*, 2017, **53**, 3781-3784.
46. C. Červinka and M. Fulem, *J. Chem. Theory Comput.*, 2017, **13**, 2840-2850.
47. A. Maiti, L. A. Zepeda-Ruiz, R. H. Gee and A. K. Burnham, *J. Phys. Chem. B*, 2007, **111**, 14290-14294.

48. K. K. Irikura and D. J. Frurip, *Computational Thermochemistry: Prediction and Estimation of Molecular Thermodynamics*, American Chemical Society, Washington, DC, 1998.
49. A. L. L. East and L. Radom, *J. Chem. Phys.*, 1997, **106**, 6655-6674.
50. J. Pfaendtner, X. Yu and L. J. Broadbelt, *Theor. Chem. Acc.*, 2007, **118**, 881-898.
51. S. Grimme, S. Ehrlich and L. Goerigk, *J. Comput. Chem.*, 2011, **32**, 1456-1465.
52. G. J. H. van Nes and A. Vos, *Acta Crystallogr. B*, 1978, **34**, 1947-1956.
53. M. T. Kirchner, D. Das and R. Boese, *Cryst. Growth Des.*, 2008, **8**, 763-765.
54. A. Budzianowski and A. Katrusiak, *Acta Crystallogr. B*, 2006, **62**, 94-101.
55. D. Paliwoda, K. F. Dziubek and A. Katrusiak, *Cryst. Growth Des.*, 2012, **12**, 4302-4305.
56. J. Hafner, G. Kresse, D. Vogtenhuber and M. Marsman, *Journal*, 2014.
57. P. E. Blöchl, *Phys. Rev. B*, 1994, **50**, 17953-17979.
58. G. Kresse and D. Joubert, *Phys. Rev. B*, 1999, **59**, 1758-1775.
59. H. J. Monkhorst and J. D. Pack, *Phys. Rev. B*, 1976, **13**, 5188-5192.
60. G. J. O. Beran, S. Wen, K. Nanda, Y. Huang and Y. Heit, *Top. Curr. Chem.*, 2014, **345**, 59-93.
61. Y. Heit and G. J. O. Beran, *J. Comput. Chem.*, 2014, **35**, 2205–2214.
62. S. Wen and G. J. O. Beran, *J. Chem. Theory Comput.*, 2011, **7**, 3733-3742.
63. J. W. Ponder, C. Wu, P. Ren, V. S. Pande, J. D. Chodera, M. J. Schnieders, I. Haque, D. L. Mobley, D. S. Lambrecht, R. A. DiStasio, M. Head-Gordon, G. N. I. Clark, M. E. Johnson and T. Head-Gordon, *J. Phys. Chem. B*, 2010, **114**, 2549-2564.
64. K. D. Nanda and G. J. O. Beran, *J. Chem. Phys.*, 2012, **137**, 174106.
65. J. W. Ponder, *Tinker 6.2*, 2013.
66. F. D. Murnaghan, *Proc. Natl. Acad. Sci. U.S.A.*, 1944, **30**, 244-247.
67. A. Halkier, T. Helgaker, P. Jorgensen, W. Klopper, H. Koch, J. Olsen and A. K. Wilson, *Chem. Phys. Lett.*, 1998, **286**, 243-252.
68. J. Řezáč and P. Hobza, *J. Chem. Theory Comput.*, 2013, **9**, 2151-2155.
69. M. S. Marshall and C. D. Sherrill, *J. Chem. Theory Comput.*, 2011, **7**, 3978-3982.
70. L. A. Burns, M. S. Marshall and C. D. Sherrill, *J. Chem. Phys.*, 2014, **141**, 234111.
71. M. Pitoňák and A. Heßelmann, *J. Chem. Theory Comput.*, 2010, **6**, 168-178.
72. J. Řezáč, C. Greenwell and G. J. O. Beran, *J. Chem. Theory Comput.*, 2018, **14**, 4711-4721.
73. H.-J. Werner, P. J. Knowles, G. Knizia, F. R. Manby and M. Schütz, *Wiley Interdiscip. Rev.: Comput. Mol. Sci.*, 2012, **2**, 242-253.
74. M. F. Peintinger, D. V. Oliveira and T. Bredow, *J. Comput. Chem.*, 2013, **34**, 451-459.
75. R. Dovesi, A. Erba, R. Orlando, C. M. Zicovich-Wilson, B. Civalleri, L. Maschio, M. Rérat, S. Casassa, J. Baima, S. Salustro and B. Kirtman, *Wiley Interdiscip. Rev.: Comput. Mol. Sci.*, 2018, **8**, e1360.
76. D. Bucker and W. Wagner, *J. Phys. Chem. Ref. Data*, 2006, **35**, 205-266.
77. J. Regnier, *J. Chim. Phys. Phys. Chim. Biol.*, 1972, **69**, 942-&.
78. H. G. Carlson and E. F. Westrum, *J. Chem. Phys.*, 1971, **54**, 1464-&.
79. S. Lucas, D. Ferry, B. Demirdjian and J. Suzanne, *J. Phys. Chem. B*, 2005, **109**, 18103-18106.
80. K. Růžička, M. Fulem and C. Červinka, *J. Chem. Thermodyn.*, 2014, **68**, 40-47.
81. H. G. M. De Wit, C. G. De Kruif and J. C. Van Miltenburg, *J. Chem. Thermodyn.*, 1983, **15**, 891-902.
82. H. G. M. De Wit, J. C. Van Miltenburg and C. G. De Kruif, *J. Chem. Thermodyn.*, 1983, **15**, 651-663.
83. P. Jimenez, M. V. Roux, C. Turrion and F. Gomis, *J. Chem. Thermodyn.*, 1987, **19**, 985-992.
84. A. Tooru and C. Hideaki, *Chem. Lett.*, 1976, **5**, 683-688.

85. F. Pavese, *J. Chem. Thermodyn.*, 1978, **10**, 369-379.
86. G. D. Oliver, M. Eaton and H. M. Huffman, *J. Am. Chem. Soc.*, 1948, **70**, 1502-1505.
87. J. H. Schachtschneider and R. G. Snyder, *Spectrochim. Acta*, 1963, **19**, 117-168.
88. E. Hirota, S. Saito and Y. Endo, *J. Chem. Phys.*, 1979, **71**, 1183-1187.
89. A. Serrallach, R. Meyer and H. H. Gunthard, *J. Mol. Spectrosc.*, 1974, **52**, 94-129.
90. E. Herbst, J. K. Messer, F. C. De Lucia and P. Helminger, *J. Mol. Spectrosc.*, 1984, **108**, 42-57.
91. M. Majoube and G. Vergoten, *J. Mol. Struct.*, 1992, **266**, 345-352.
92. W. B. Nelligan, D. J. Lepoire, T. O. Brun and R. Kleb, *J. Chem. Phys.*, 1987, **87**, 2447-2456.
93. M. G. Wisnosky, D. F. Eggers, L. R. Fredrickson and J. C. Decius, *J. Chem. Phys.*, 1983, **79**, 3505-3512.
94. O. Galvez, B. Mate, B. Martin-Llorente, V. J. Herrero and R. Escribano, *J. Phys. Chem. A*, 2009, **113**, 3321-3329.
95. A. Anderson, B. Andrews, E. M. Meiering and B. H. Torrie, *J. Raman Spectrosc.*, 1988, **19**, 85-89.
96. E. R. Bernstein, *J. Chem. Phys.*, 1970, **52**, 4701-4716.
97. G. Taddei, H. Bonadeo, M. P. Marzocchi and S. Califano, *J. Chem. Phys.*, 1973, **58**, 966-978.
98. J. P. Pinan, R. Ouillon, P. Ranson, M. Becucci and S. Califano, *Journal of Chemical Physics*, 1998, **109**, 5469-5480.
99. P. W. Loeffen, R. F. Pettifer, F. Fillaux and G. J. Kearley, *J. Chem. Phys.*, 1995, **103**, 8444-8455.
100. C. Perchard and A. Novak, *J. Chem. Phys.*, 1968, **48**, 3079-3084.
101. M. Majoube and G. Vergoten, *J. Chem. Phys.*, 1982, **76**, 2838-2847.
102. K. E. Riley, M. Pitoňák, P. Jurečka and P. Hobza, *Chem. Rev.*, 2010, **110**, 5023-5063.

Table of contents

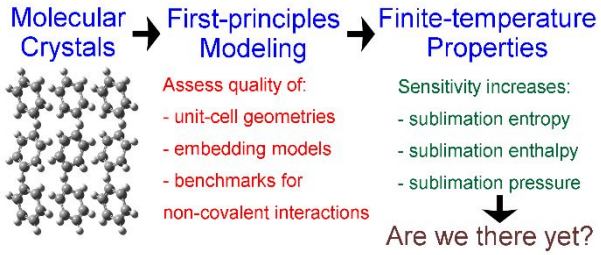

Synopsis

State-of-the-art *ab initio* predictions of sublimation pressures, matching experiment to a factor of 2-10, outperform the reliability of empirical estimates.